Postprint of: Oad V. K., Szymkiewicz A., Khan N. A., Ashraf S., Nawaz R., Elnashar A., Saad S., Qureshi A. H., Time series analysis and impact assessment of the temperature changes on the vegetation and the water availability: A case study of Bakun-Murum Catchment Region in Malaysia, Remote Sensing Applications: Society and Environment, Vol. 29 (2023), 100915, DOI: 10.1016/j.rsase.2022.100915

Time series analysis and impact assessment of the temperature changes on the vegetation and the water availability: A case study of Bakun-Murum Catchment Region in Malaysia

Vipin Kumar Oad[1*], Adam Szymkiewicz[1], Nabeel Ali Khan[2], Shahzad Ashraf[3], Rab Nawaz[4], Abdelrazek Elnashar[5], Syed Saad[6], and Abdul Hannan Qureshi[6]

[1]Faculty of Civil and Environmental Engineering, Gdańsk University of Technology, 80-233 Gdańsk, Poland

[2]Pakistan Council of Research in Water Resources Regional Office, PCRWR, Main University Road, Near KW&SB Reservoir, Gulistan-e-Johar, Block-1, Karachi 75290, Pakistan

[3]Department of Mechanics of Materials and Structures, Faculty of Civil and Environmental Engineering, Gdańsk University of Technology, Narutowicza 11/12, 80-233, Gdańsk, Poland

[4]Fundamental and Applied Sciences Department (FASD), Universiti Teknologi PETRONAS, Seri Iskandar 32610, Perak, Malaysia

[5]Department of Natural Resources, Faculty of African Postgraduate Studies, Cairo University, Giza 12613, Egypt

[6]Department of Civil and Environmental Engineering, Universiti Teknologi Petronas, Tronoh, Perak, 32610, Malaysia

[*]Corresponding author: vipin.oad@pg.edu.pl

Abstract

The Bakun-Murum (BM) catchment region of the Rajang River Basin (RRB), Sarawak, Malaysia, has been under severe threat for the last few years due to urbanization, global warming, and climate change. The present study aimed to evaluate the time series analysis and impact assessment of the temperature changes on the vegetation/agricultural lands and the water availability within the BM region. For this purpose, the Landsat data for the past thirty years (1990-2020) were used. Remote sensing techniques for estimating the surface temperatures and variation within the vegetation and water bodies were utilized, and validation was done using on-ground weather stations. Google Earth Engine (GEE) and other RS & GIS tools were used for analyzing the time series trends of land surface temperature (LST), normalized difference vegetation index (NDVI), and normalized difference water index (NDWI). The results exposed an overall rise of 1.06°C in the annual mean temperatures over the last thirty years. A maximum annual mean NDVI of 0.48 was recorded for 2018 and 2019. The lowest annual mean NDVI (0.27) was observed in 2005. The annual mean NDWI increased to 0.48 in 2018 and 2019, respectively. The statistical correlation results revealed the coefficient of determination (R^2) of 0.09 and 0.13 for the annual mean LST and annual mean NDVI and the annual mean LST and annual mean NDWI, respectively. Moreover, the Mann-Kendall trend test for the annual mean temperature series indicates a slightly increasing trend

with Sen's slope of 0.03°C/year. It is found that there is a positive trend in the annual mean rainfall patterns, as Sen's slope indicates a yearly increase of 50.58 mm/year. This study found significant changes in the LST, NDVI, and NDWI of the BM catchment region during the last thirty years, demanding the concerned authorities' instant attention to alleviate the adverse effects of such changes to protect the ecosystem.

Keywords: Time series analysis; google earth engine; remote sensing & GIS; impact assessment; land surface temperature

1. Introduction

The LST usually determines the current urban environment's ecological health (Patz et al., 2005; Grimm et al., 2008; Huang et al., 2009; Du et al., 2016; Liu et al., 2018; Oad et al., 2020). Urbanization is a fast human-induced process primarily based on urban area expansion, and land transformation (Guha et al., 2020) has not only decreased the agricultural lands and contributed to the increased temperature. The remote-sensing normalized difference indices are usually used to identify ecological shifts within natural resources (Chen et al., 2006; Govil et al., 2019; He et al., 2019; Govil et al., 2020; Guha et al., 2020). Remote sensing also provides the TIR structure of the wavelengths, which is also very useful in assessing the variability of LST temporally and spatially. Remote sensing is widely implemented in every field of earth science (Wen et al., 2017; Ferrelli et al., 2018; Alexander, 2020; Nimish et al., 2020; Sultana & Satyanarayana, 2020). The spatial heterogeneity of the LST is due to the variation in roughness and reflectance of the ground surface (Grimm et al., 2008). The LST has risen due to global climate change impacts on the meteorological parameters, affecting water resources, land cover, land use, and vegetated areas. It is claimed that different environmental problems are responsible for such changes (Chan & Yao, 2008; Choudhury et al., 2019). Using satellite imagery, shortwave infrared (SWIR), visible and near-infrared (VNIR), and thermal infrared (TIR) bands allow us to monitor ecological changes (Chan & Yao, 2008; Mondal et al., 2011; Das et al., 2013; Alexander, 2020). Land surface temperature represents the Earth's surface temperature and is one of the critical parameters that influence surface-energy balance, heat fluxes, energy exchanges, and regional climates (Wan & Dozier, 1996; Dash et al., 2002; Karnieli et al., 2010; Meng et al., 2017; Fang et al., 2018; Zhou et al., 2018; Martin et al., 2019).

The effects of LST on various subjects have been investigated by several researchers, including surface heat island (SHI), geological and geothermal studies (Coolbaugh et al., 2007;

Eskandari et al., 2015; Mia et al., 2018; Sekertekin & Arslan, 2019), evapotranspiration (Elnashar et al., 2021), forest fire monitoring (Maffei et al., 2018), and urban climate studies (Sekertekin et al., 2016; Naughton & McDonald, 2019; Simwanda et al., 2019). LST has also been acknowledged as one of the essential criteria for the International Geosphere and Biosphere Program (IGBP) (Townshend et al., 1994; Li et al., 2013). Meteorological stations estimate air Temperatures from radiance measurements. However, as it is a point-based measurement, it does not necessarily allow extensive monitoring on a larger scale (Hale et al., 2011). On the other hand, remotely sensed TIR data enables large-scale, even global, temporal, and spatial LST observation (Gao et al., 2013). It is crucial for meteorologists, agronomists, and hydrologists to know the different terms that interact with the surface energy balance. The LST, however, is one of the key parameters that play a significant role in the interaction processes of the atmosphere, hydrosphere, and biosphere (Douglas & Aochi, 2008). The LST is also used throughout many fields, such as the hydrological cycle, evapotranspiration, vegetation, climate change, etc. (Douglas & Aochi, 2008). It is the critical factor influenced by the properties of the Earth's surface, such as landscape, land cover, vegetation, land usage, and permeability of the soil surface (Khandelwal et al., 2018). Many studies have been conducted to detect LST variations because of land use, vegetation, and land cover differences. Most research studies (Chan & Yao, 2008; Choudhury et al., 2019) have reported a negative correlation between natural vegetation and LST, referring to the reduction of LST in crop cover. The LST can be quantified using the traditional method and remote sensing (RS) technique. The LST is determined through meteorological stations as temperature using traditional methods, whereas RS allows assessing it through the energy balance's surface model (Daou et al., 2012). It is suggested that LST is a vital microclimate variable and that radiation is transmitted within the atmosphere. Remote sensing and geographical information system tools, alongside ground-truthing data collected, are suggested for evaluating the spatiotemporal changes in the LST.

Various vegetation indexes are known to examine differences in the vegetative zone. Among the most accurate, most extensive, and most widely used indexes is NDVI (Sruthi & Aslam, 2015). It is possible to calculate the changes in vegetation in a specific area using NDVI. Several researchers using GIS and Remote Sensing techniques are currently exploring the inverse relationship between LST and NDVI (Chen et al., 2010). Researchers identified that satellite imagery thermal bands can calculate the LST (Dagliyar et al., 2015). Using the OLI/TIRS data acquired, Dagliyar et al., 2015 identified the LST in Erzurum, Turkey.

Rajendran et al., 2015 focused on LST using the Landsat 8 thermal bands; OLI/TIRS images show that LST is a feature of vegetative cover and soil water content in India. Using satellite data, Crawford et al., 2006 observed the relationships between NDVI and LST in China's Shanghai region. It stated that GIS and RS techniques helped determine the climate change impacts on the ecosystem. Rapid changes in land use and land cover patterns have resulted in major LST shifts.

The normalized difference water index (NDWI) is the most common index for surface water abstraction that is often implemented in land use and LST-related analyses (Yuan et al., 2017). In addition, the nature of the LST-NDWI relationship is not linear and marginal in an urban climate. Temperature, precipitation, plants, barren land, environmental effluence, warm or cold soil, an organic layer, various human-made products, and other influences affect it (McFeeters, 1996; Ghobadi et al., 2015). NDWI and LST's relationship has been established using TIR remote sensing in various current research studies (Chen et al., 2006; Choudhury et al., 2019; Govil et al., 2019; Solangi et al., 2019). But, in subtropical Malaysia, the seasonal study of the LST-NDWI relationship is unusual. Owing to the seasonal variations in air temperature, moisture content, precipitation, evaporation, etc., NDWI and LST's nature has changed. Consequently, in Malaysia's subtropical climate, a constant evaluation of the LST-NDWI relation is crucial (Hussain et al., 2018).

The study focused on evaluating the impact of variations in the LST on vegetation and water bodies and assessing the correlations between them for the Bakun-Murum catchment region in Sarawak, Malaysia. The Bakun-Murum region was selected because it has been severely affected by climatic conditions. The following specific objectives achieved the primary goal:

- Firstly, the data was collected from the respective repositories and departments. Secondly, the satellite data were analyzed using the Google Earth Engine code editor to determine the trends in the LST, NDVI, and NDWI.
- Finally, XLSTAT and R statistical tools were used for the Pearson correlation analysis of annual mean LST with mean NDVI, annual mean NDWI, annual mean temperature, and annual mean rainfall.

Due to the limitations and unavailability of cloud-free Landsat satellite imageries for the selected years, we conducted this study using GEE as the available Landsat data specifically for the BM region is of no use because of the cloud covers. The results of this research would

be helpful for future urban and country planners, policymakers, environmentalists, and farmers in the region to take remedial steps to reduce the impacts of climate change in the study area.

2. Materials and Methods

2.1 The Study Area

Figure 1 shows the location map of the study area developed with the help of the shapefiles and digital elevation model (DEM) using ArcGIS 10.8. The required shapefiles for the study area map were created using Google Earth Pro, and the administrative boundaries shapefile of Malaysia was downloaded from DIVA-GIS http://www.diva-gis.org/download.

Malaysia's Sarawak state is covered by thick tropical rainforests and is rich in water resources (Hussain et al., 2018). It also has a perfect hydropower development landscape (Hussain et al., 2018). Sarawak is located at 1.5533° N, and 110.3592° E. The Southwestern monsoon (May to September) and the North-easterly monsoon (October to April) are the two monsoon seasons in Sarawak (Hussain et al., 2018). In this region, the Southwestern monsoon has less rainfall than the Northeastern monsoon (Hussain et al., 2018). The minimum rainfall periods are June to August, and the months from December to February are the rainiest each year (Hussain et al., 2018). Throughout Malaysia's Sarawak state, the Rajang River Basin (RRB) is the primary river in agricultural and economic development (Hussain et al., 2018). RRB is located on Borneo Island (2.1245° N, 111.2181° E), the largest island in Asia and the third largest island worldwide. It drains fifty thousand square kilometres of Sarawak's tropical rainforest, accounting for 40% of the state's total area (Oad et al., 2020). In the RRB area, annual precipitation varying from 3000 to 5200 millimetres is plentiful, and the river is very well recognized for the hazards of high soil erosion (Hussain et al., 2018). In the upper portion of the RRB, the catchment elevations range from sea level to about 2016 meters on the west coast. This river is the largest in Malaysia, with an overall length of 563 kilometres. RRB originated from the mountains of Iran (Nakisa et al., 2014; Hussain et al., 2018).

The geographical features of the study area are shown in Figure 2, including slope (Figure 2a), aspect ratio (Figure 2b), and hillshade (Figure 2c). They were evaluated from the Shuttle Radar Topography Mission (SRTM) 1 Arc-Second Global digital elevation model (DEM) of a 30 m by 30 m resolution. The DEM was downloaded from the USGS Earth Explorer https://earthexplorer.usgs.gov/. A slope map shows a region's topography and an overview of topographical characteristics that have affected and may continue to impact land creation (Oad et al., 2020). The slope of the study area ranged from 7.48% to 63.59% in figure

2(a). The aspect and degree of slope for the study area are shown simultaneously by an aspect-ratio map in figure 2(b). Hues (e.g., orange, yellow, red, etc.) symbolize aspect groups, and the degree of slope classes are mapped with saturation such that the steeper ones are lighter. Hillshading is a method for making relief maps; shading (points of grey) displays the topographical form of hills and mountains, suggesting relative slopes and mountain edges, not total height. A topographical map showing the contour lines of the shape of the ground's surface, the comparative space of the lines representing the surface's relative angle.

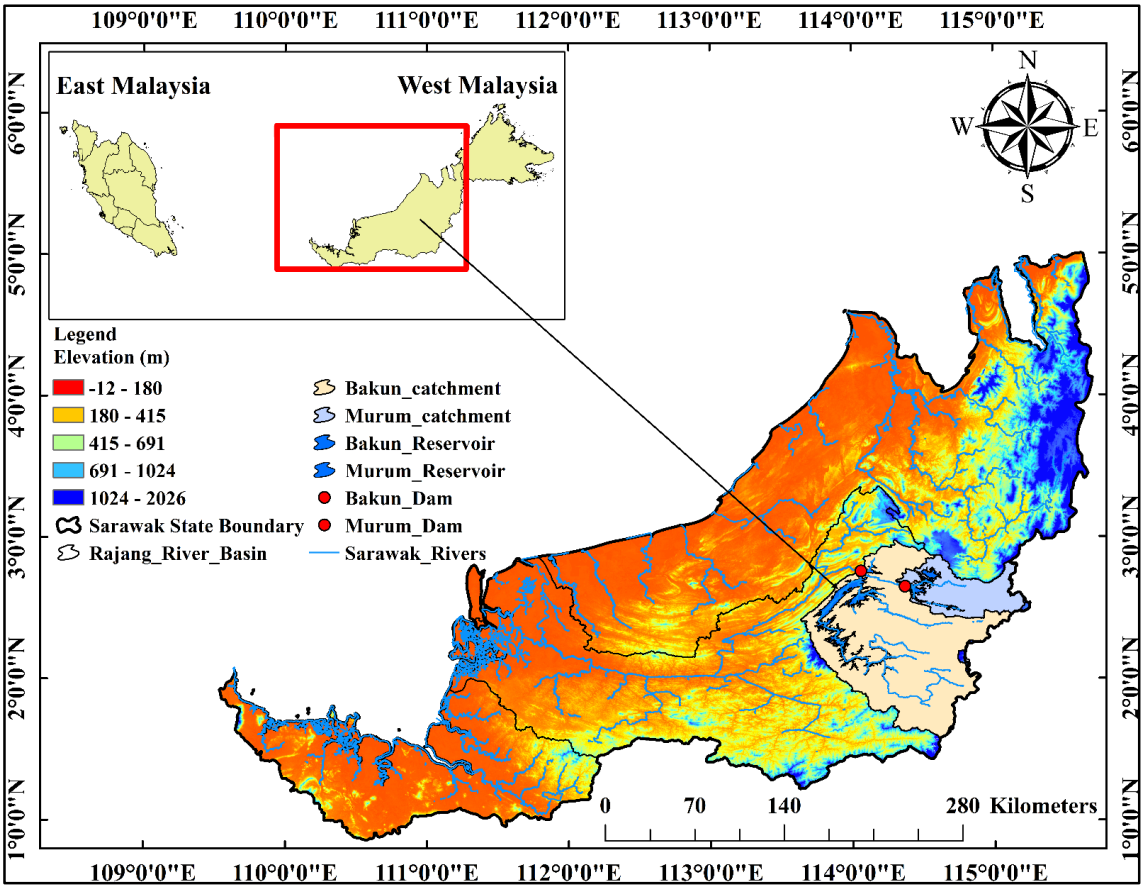

Figure. 1. Map of the study area.

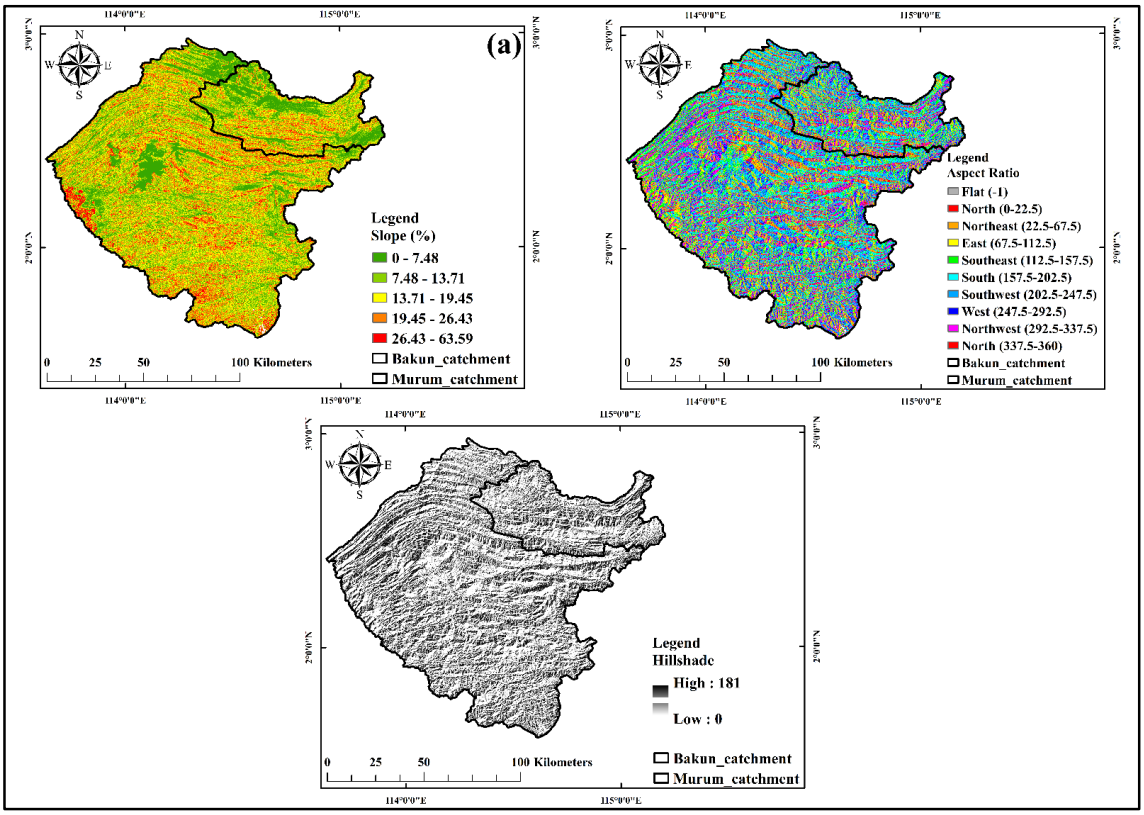

Figure. 2. Geological features of the study area (a) slope, (b) aspect ratio, and (c) hillshade.

2.2 Description of Datasets

Google Earth Engine code editor (https://code.earthengine.google.com/) was used to acquire the level 2 surface reflectance of Landsat 5 and 8 images from 1990 to 2020. Only cloud-free images (less than 10% clouds) were processed. As discussed in the later sections, the respective bands from each image were later used in the estimation of NDVI and NDWI. The description of the datasets may be obtained from https://developers.google.com/earth-engine/datasets/catalog/landsat.

2.3 Land Surface Temperature

LST was estimated by using an open-source code developed and described by Ermida et al., (2020) to estimate the LST from the Landsat series and ASTER emissivity using the GEE code editor. The script to calculate the LST using GEE is attached at https://code.earthengine.google.com/cbc91b8ed4af97453106b5bacc003970?accept_repo=users%2Fvipinkoad%2FRSPaper.

2.4 Determination of Vegetation Cover

The normalized difference vegetation index (NDVI) was evaluated using the GEE code editor to determine the temporal changes in the vegetative cover. This index was determined using the NIR (near-infrared) and red (R) bands, as described in Equation 1 (Choudhury et al., 2019). Numerous scholars worldwide have used this index as an indicator of green vegetation. For Landsat 5, bands 3 and 4 were used, but for Landsat 8/OLI, bands 4 and 5 were used to calculate NDVI. The index's values vary from -1 to +1. A value of -1 represents a non-vegetated area, while +1 indicates a vegetative area (Yuan et al., 2017). The script to estimate the NDVI using GEE is attached at https://code.earthengine.google.com/e2c4d973d24e8c4a672631647252dfc3?accept_repo=users%2Fvipinkoad%2FRSPaper.

$$\mathrm{NDVI} = \frac{\mathrm{NIR} - \mathrm{R}}{\mathrm{NIR} + \mathrm{R}} \quad (1)$$

2.5 Determination of Water Index

The normalized difference water index (NDWI) was used as a stable normalized difference spectral index in the current research analysis to test the correlation of water bodies with LST. The NDWI defined in Equation 2 (McFeeters, 1996; McFeeters, 2013) was calculated using green (G) and near-infrared (NIR) bands. For the TM data, band two was used as a green band, and band four was used as the NIR band, comparatively. For OLI/TIRS data, bands 3 and 5 were used as green and NIR, respectively. The NDWI value ranges from -1 to +1 (Yuan et al., 2017). A negative NDWI value implies that there are no water bodies in the region and that the land is dry, while a positive NDWI value indicates water surfaces and plants. The google earth engine script to estimate the NDWI is attached at https://code.earthengine.google.com/888ef20dfacb8076d39e0f397064d132?accept_repo=users%2Fvipinkoad%2FRSPaper.

$$\mathrm{NDWI} = \frac{\mathrm{G} - \mathrm{NIR}}{\mathrm{G} + \mathrm{NIR}} \quad (2)$$

2.6 Climate Data

The meteorological data for Malaysia's Sarawak state for the years 1990 to 2020 was obtained from the Malaysian Meteorological Department. The data are the annual mean temperature in degrees Celsius (°C) and the annual mean rainfall in millimetres (mm). The annual mean temperature and annual mean rainfall series data were analyzed for trend interpretation and

shifts in the trend slope. Trend identification was achieved using the Mann-Kendall non-parametric test and Sen's estimator's trend slope. It's a distribution-free test that doesn't use normally distributed data (Ahmad et al., 2018; Arfan et al., 2019; Tayyab et al., 2019; Waseem et al., 2020). Sen's estimator lists the N values' time series from most minor to largest and computes them. Sen's slope estimator is the median of these N values (Oad et al., 2020).

2.7 Statistical Analyses

As Choudhury et al., 2019 described, the LST was integrated with NDVI and NDWI to see the influence of the LST on the vegetative cover and water resources of the Bakun-Murum catchment area of the Rajang River basin. Pearson correlation analysis was used to illustrate how the evolving LST has influenced the region's vegetative cover and water resources.

3. Results and Discussion

3.1 Dynamics of land surface temperature (LST)

Figures 3a, 3b, and 3c depict the temporal changes in the annual mean land surface temperature of the Bakun-Murum catchment area from 1990 to 2020. It was observed that the regions of water and trees have lower LST than towns and barren lands. The LST and its causative factors have realistic and empirical consequences for advanced crop growth management systems in an arid and semi-arid climate. Figure 3a shows a decrease in the LST from 19.87°C in 1990 to 17.09°C in 1999. A slight increase was found from 19.87°C in 1990 to 19.96°C in 1997. Moreover, Figure 3b showed a rise from 19.42°C in 2000 to 21.02°C in 2005, and a slight decrease was observed at 20.43°C in 2007. Furthermore, from Figure 3c, an increasing LST trend can be seen from 19.95°C in 2013 to 22.10°C in 2014. Again, a decreasing trend from 2014 to 2017 in Figure 3d was observed. From 2017 to 2019, an increasing LST was observed; from 2019 to 2020, it slightly decreased. Finally, an overall increase of 1.06°C in the mean LST has been found from 1990 to 2020 in Figure 3d.

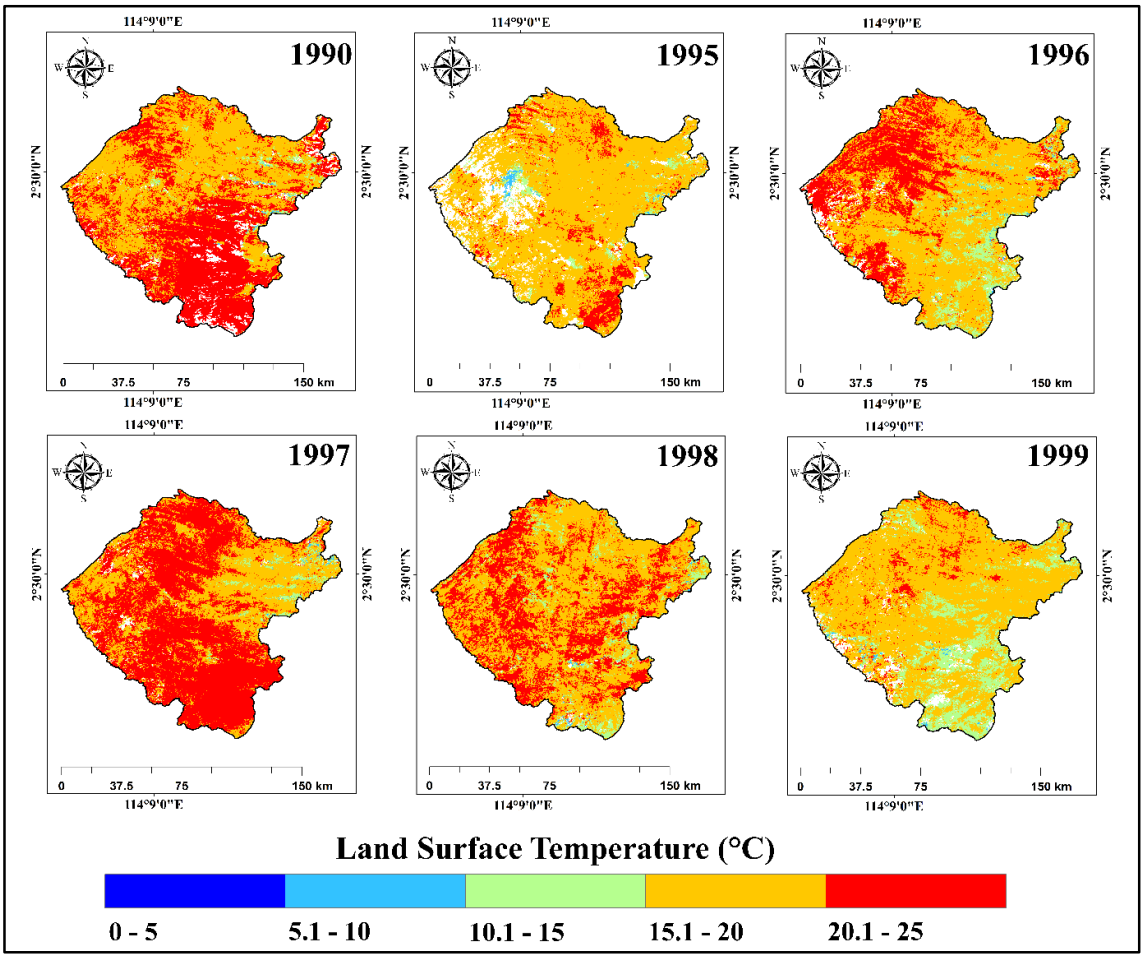

239

240 Figure. 3 (a). Temporal variations of the study area's annual mean land surface temperature

241 (1990, 1995, 1996, 1997, 1998, and 1999).

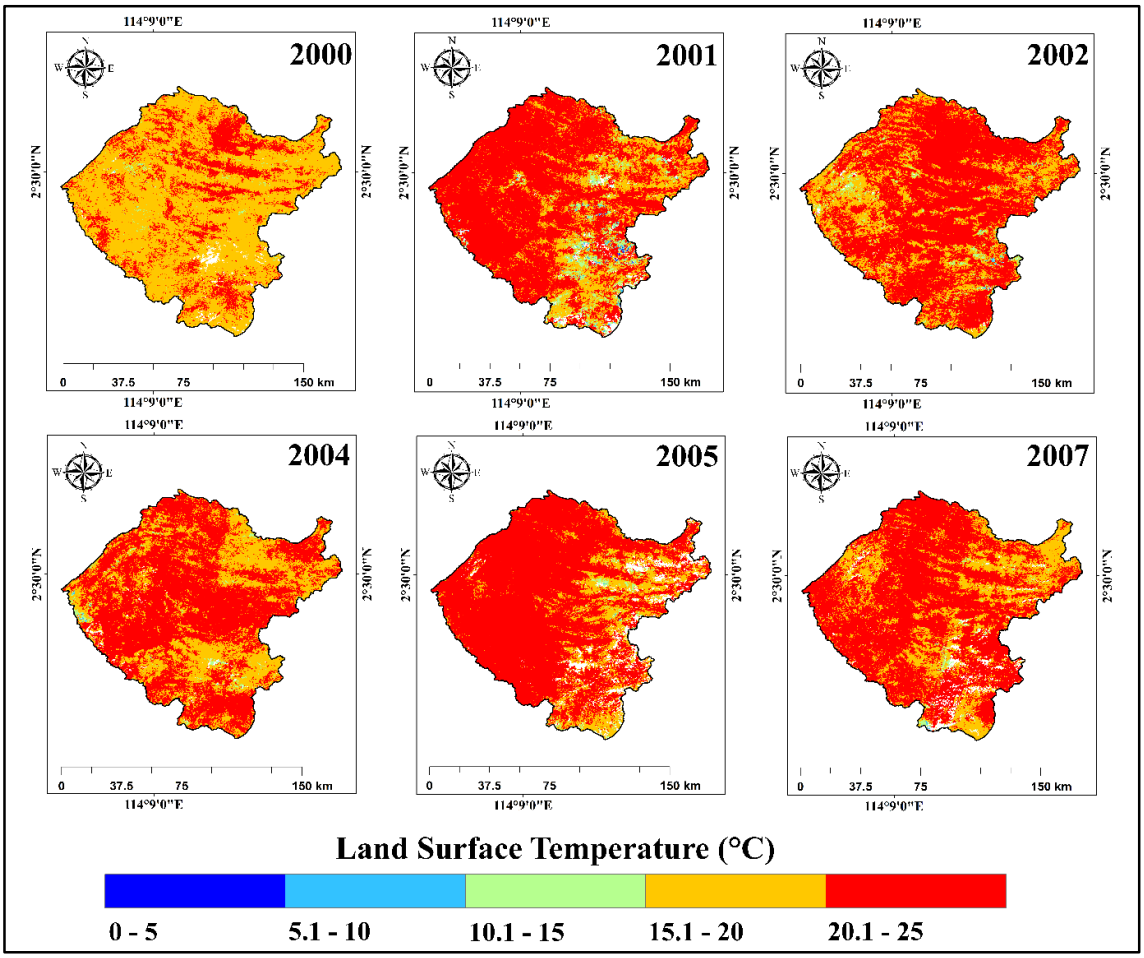

Figure. 3 (b). Temporal variations of the study area's annual mean land surface temperature (2000, 2001, 2002, 2004, 2005, and 2007).

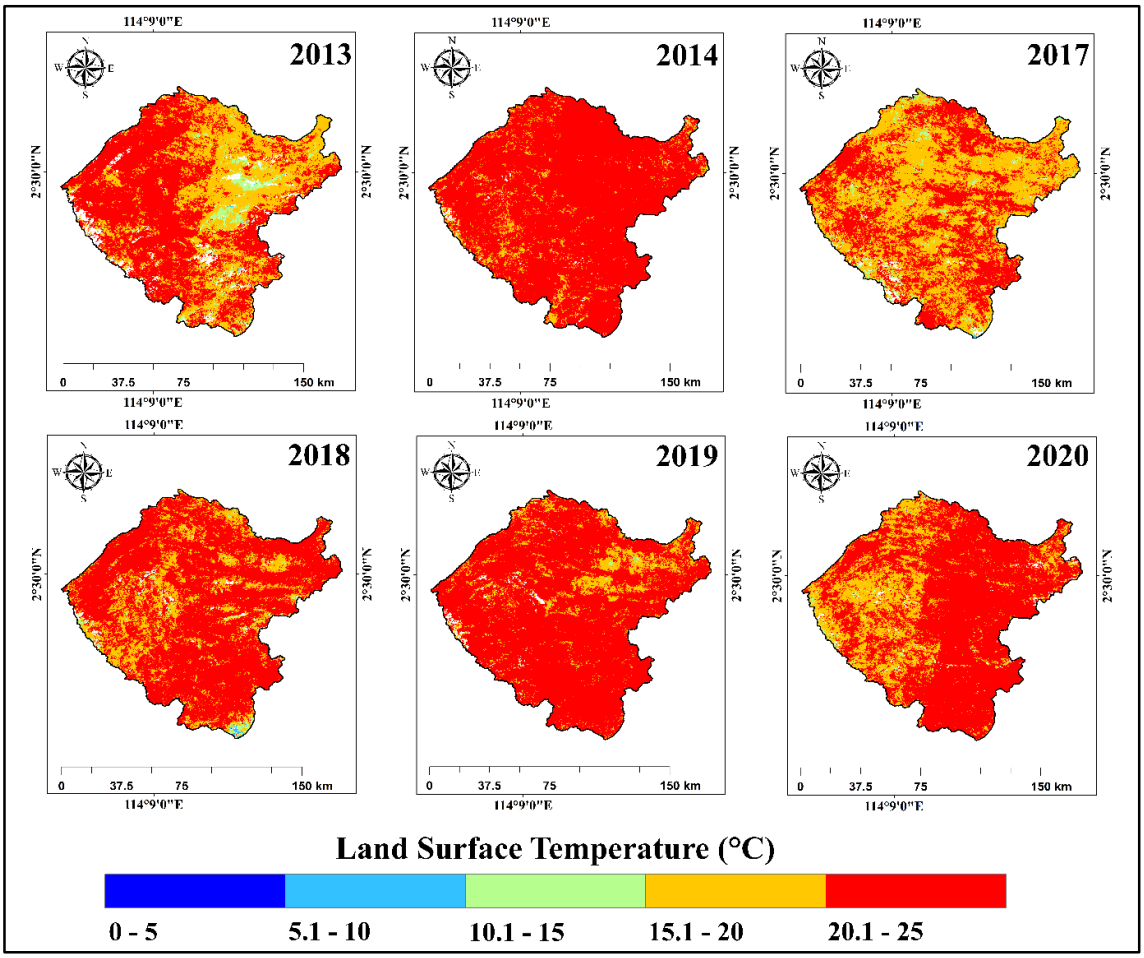

Figure. 3 (c). Temporal variations of the study area's annual mean land surface temperature (2013, 2014, 2017, 2018, 2019, and 2020).

For several factors, increasing LST patterns have a more significant impact on crop growth. Figure 3d indicates time-based changes in the LST of the study area under several ranges of temperature. Shifts in the LST are more prominent in the Rajang River Basin's Bakun-Murum catchment area. It is because of climate change and changes in the region's hydrological characteristics due to the developmental growth of the late 1990s. Several factors, such as increased housing areas and overall global climate change, can lead to a temporal increase in LST.

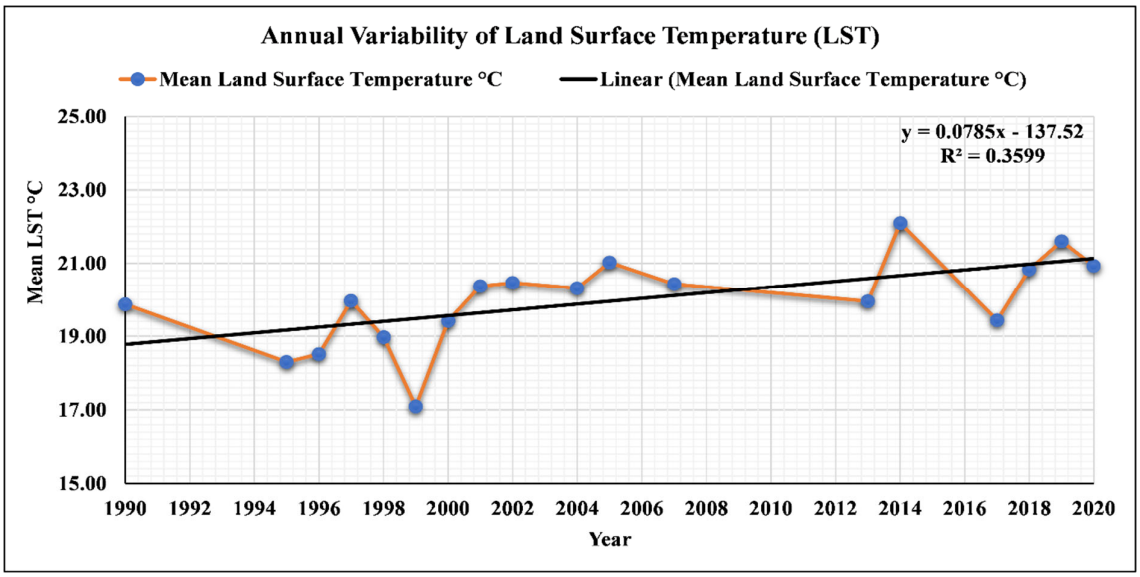

Figure. 3 (d). Annual variability of land surface temperature from 1990 to 2020.

3.2 Temporal variations in the vegetation index (NDVI)

Figures 4a, 4b, and 4c indicate chronological changes in the vegetative cover of the Bakun-Murum catchment zone. The annual variability of the annual mean normalized difference vegetation index is shown in Figure 4d. It can be observed from Figure 4a that the NDVI decreased from 0.42 in 1990 to 0.36 in 1995. From 1995 to 1996, an increase of 0.04 in NDVI was found. A decreasing trend of 0.08 NDVI was observed from 1998 to 1999. Figure 4b depicts a continuous increasing trend in the NDVI from 0.32 in 2000 to 0.38 in 2002. Moreover, a decrease of 0.11 NDVI was found from 2002 to 2005. Then from 2005 to 2007, a considerable increase was observed from 0.27 to 0.45. Furthermore, from 2007 to 2013, an increasing trend continued, while a slight decrease of 0.03 NDVI was found from 2013 to 2014; again, a rising trend continued from 2014 to 2020. Finally, an overall increase of 0.05 NDVI has been found from 1990 to 2020.

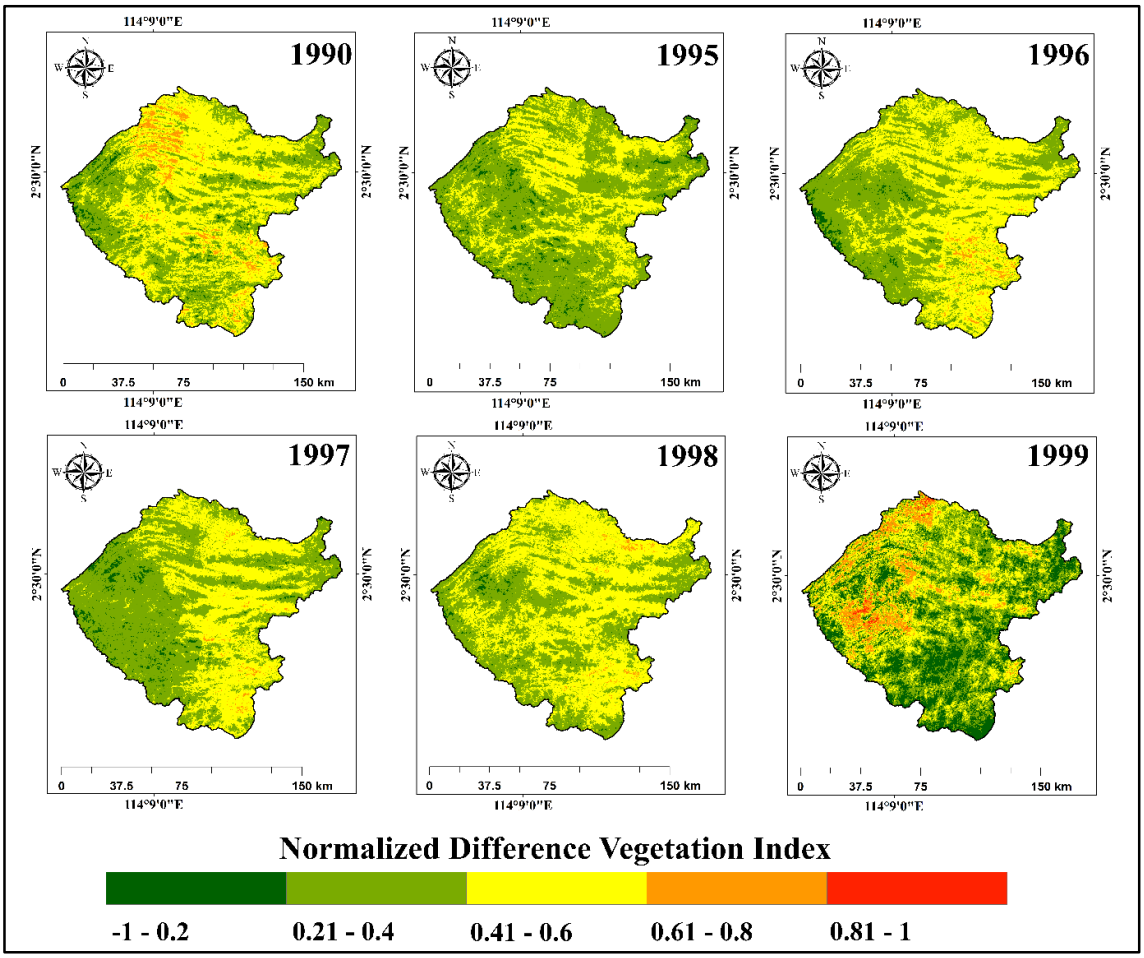

Figure. 4 (a). Temporal variations of the study area's annual mean normalized difference vegetation index (1990, 1995, 1996, 1997, 1998, and 1999).

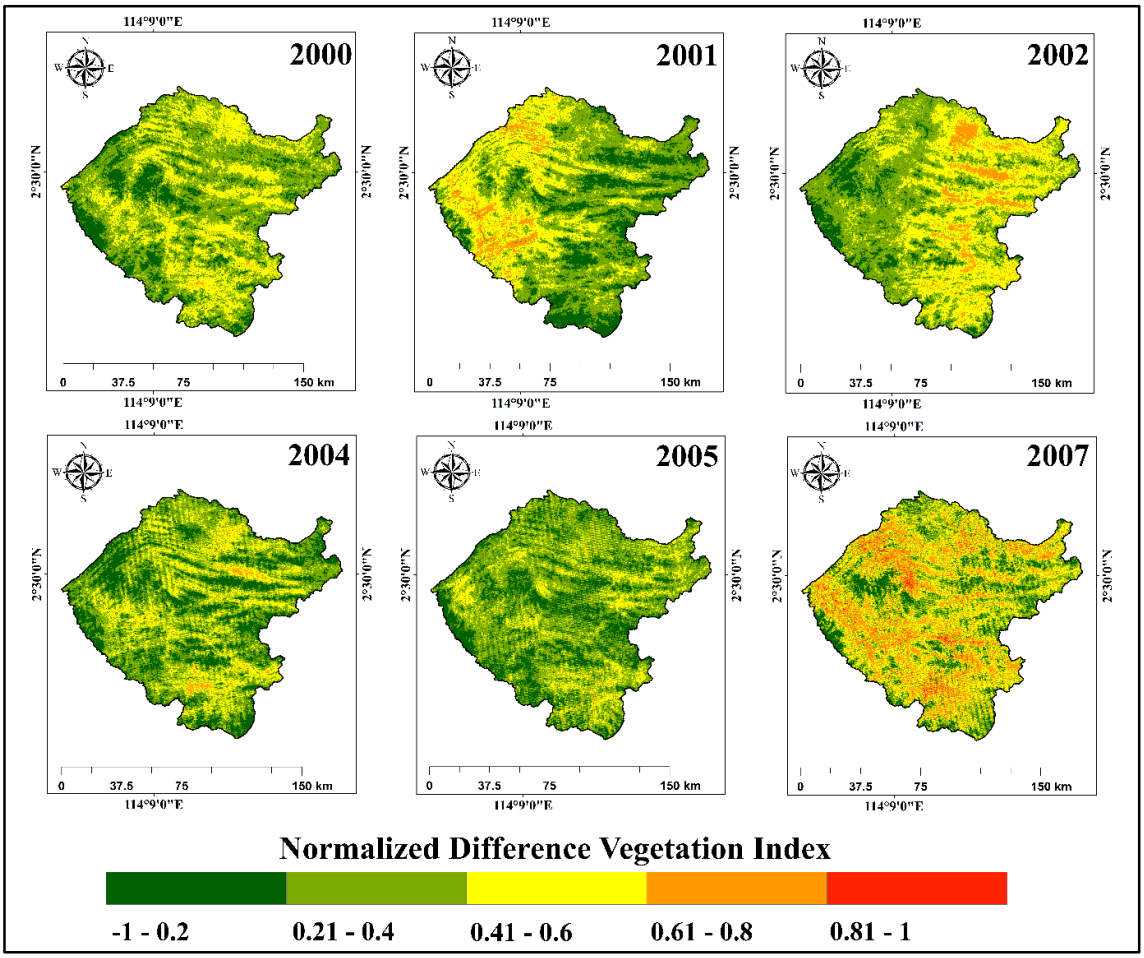

Figure. 4 (b). Temporal variations of the study area's annual mean normalized difference vegetation index (2000, 2001, 2002, 2004, 2005, and 2007).

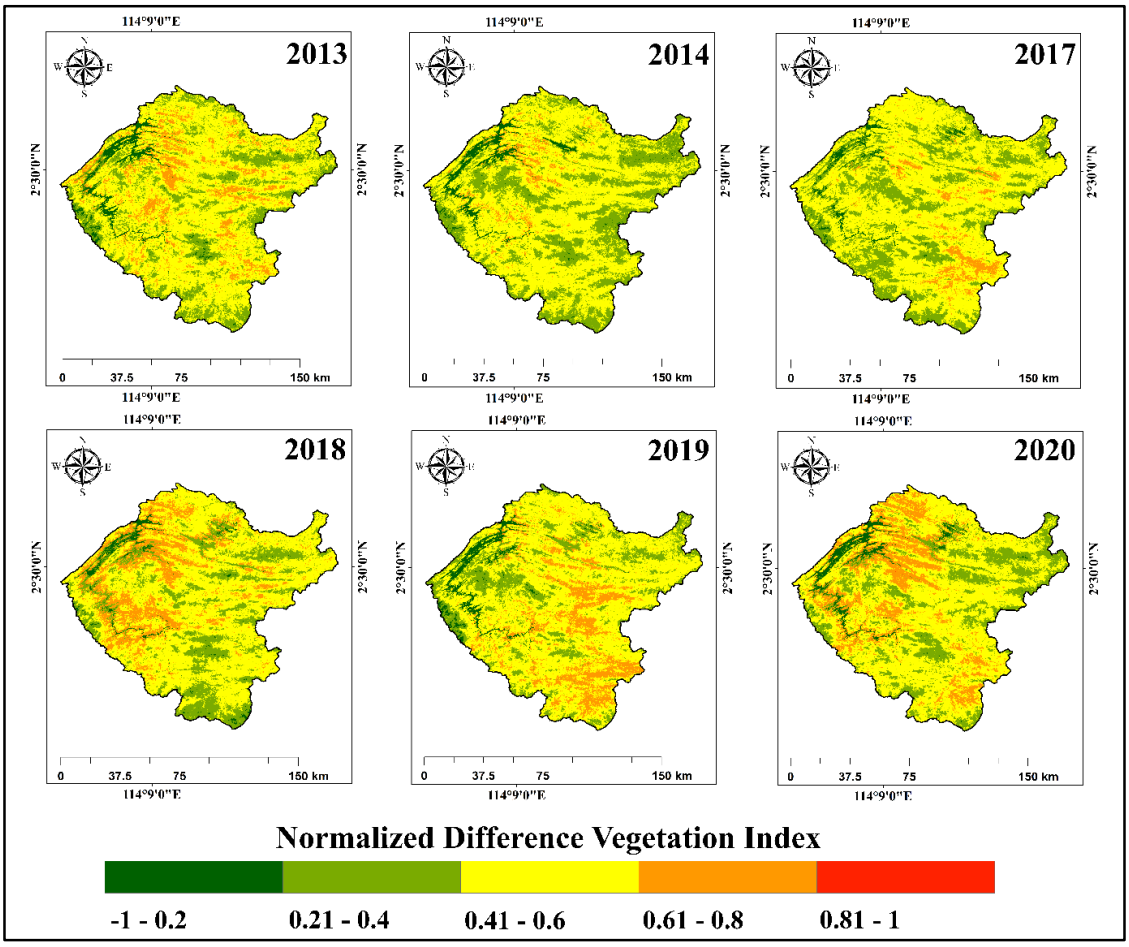

Figure 4. (c). Temporal variations of the study area's annual mean normalized difference vegetation index (2013, 2014, 2017, 2018, 2019, and 2020).

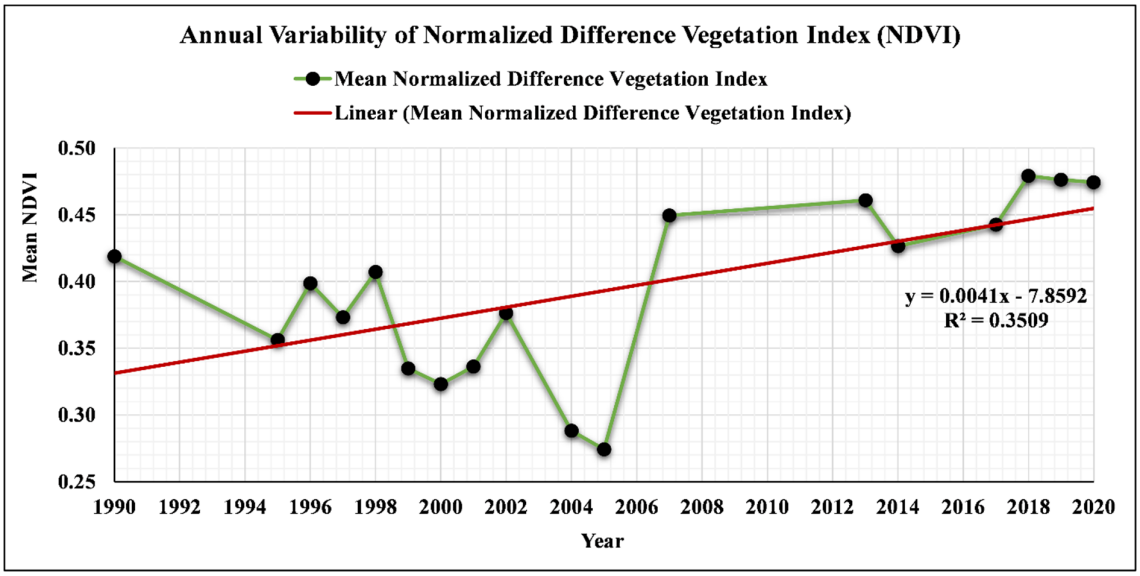

Figure. 4 (d). Annual variability of normalized difference vegetation index from 1990 to 2020.

Several factors, such as the increase in the developmental areas, increasing LST, and overall global climate change, may lead to a temporal reduction in the NDVI.

3.3 Temporal variations in the water index (NDWI)

Figures 5a, 5b, and 5c indicate sequential changes in the water bodies of the Bakun-Murum catchment zone. The annual variability of the annual mean normalized difference water index is shown in Figure 5d. It can be observed from Figure 5a that the NDWI decreased from 0.39 in 1990 to 0.34 in 1995. From 1995 to 1996, an increase of 0.04 in NDWI was found. A decreasing trend of 0.05 NDWI was observed from 1998 to 1999. Figure 5b depicts a continuous increasing trend in the NDWI from 0.32 in 2000 to 0.38 in 2002. Moreover, a decrease of 0.11 NDWI was found from 2002 to 2005. Then from 2005 to 2007, a considerable increase was observed in NDWI from 0.27 to 0.45. Furthermore, from 2007 to 2013, an increasing trend continued, while a slight decrease of 0.03 NDWI was found from 2013 to 2014; again, a rising trend continued from 2014 to 2020. Finally, an overall increase of 0.08 NDWI has been found from 1990 to 2020.

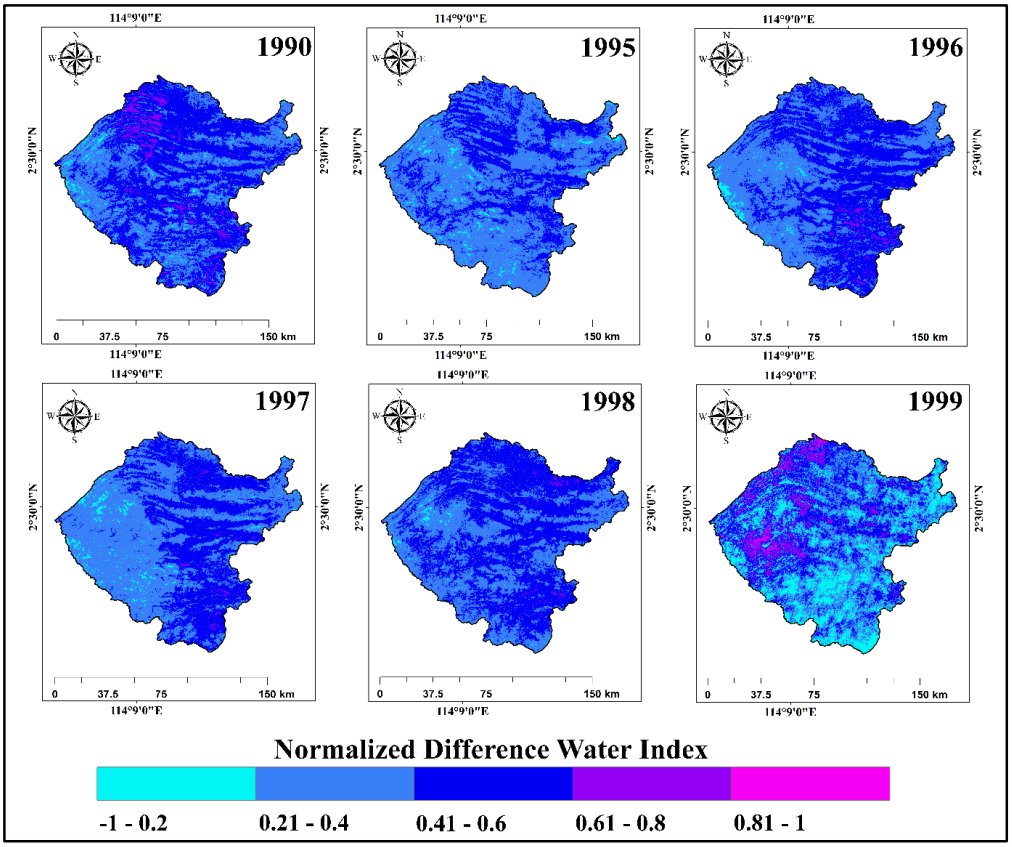

Figure. 5 (a). Temporal variations of the study area's annual mean normalized difference water index (1990, 1995, 1996, 1997, 1998, and 1999).

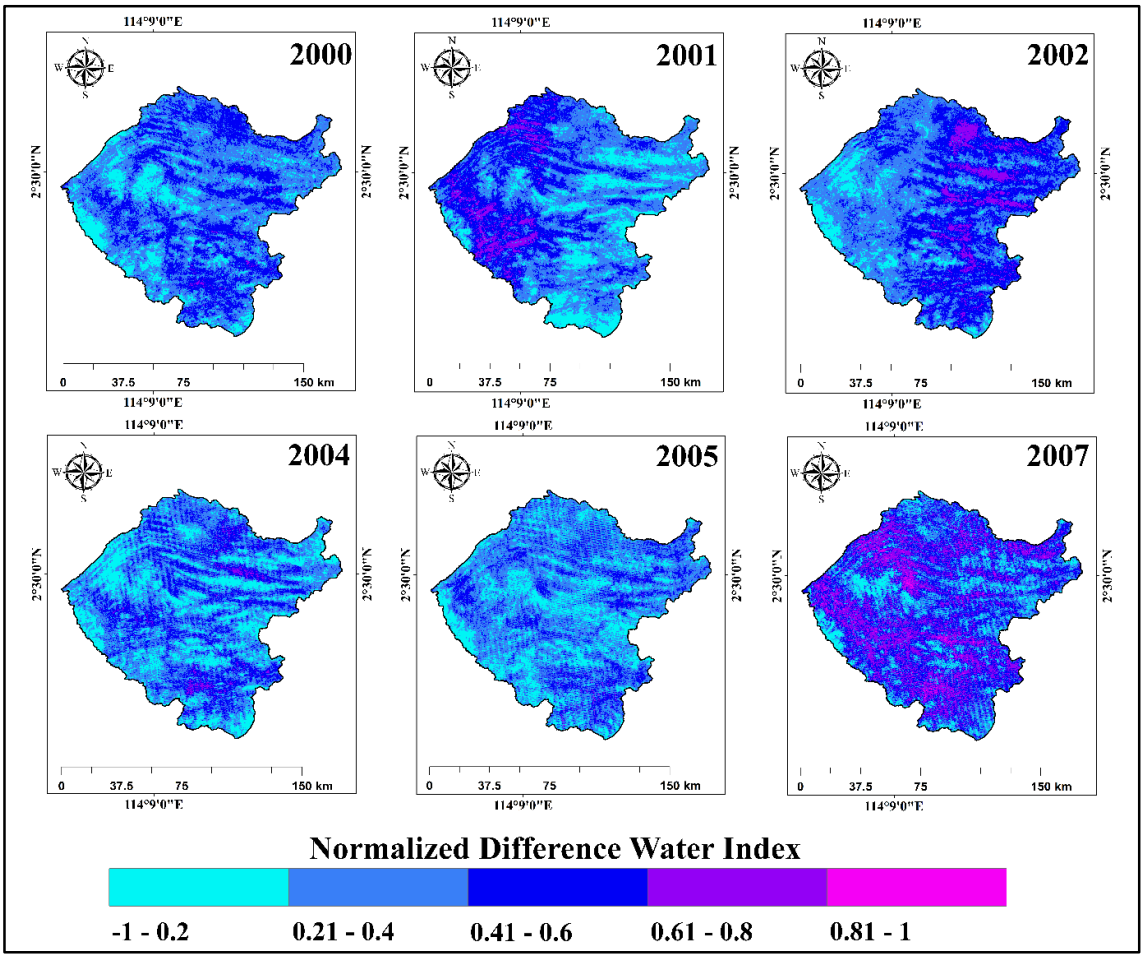

298

299 Figure. 5 (b). Temporal variations of the study area's annual mean normalized difference

300 water index (2000, 2001, 2002, 2004, 2005, and 2007).

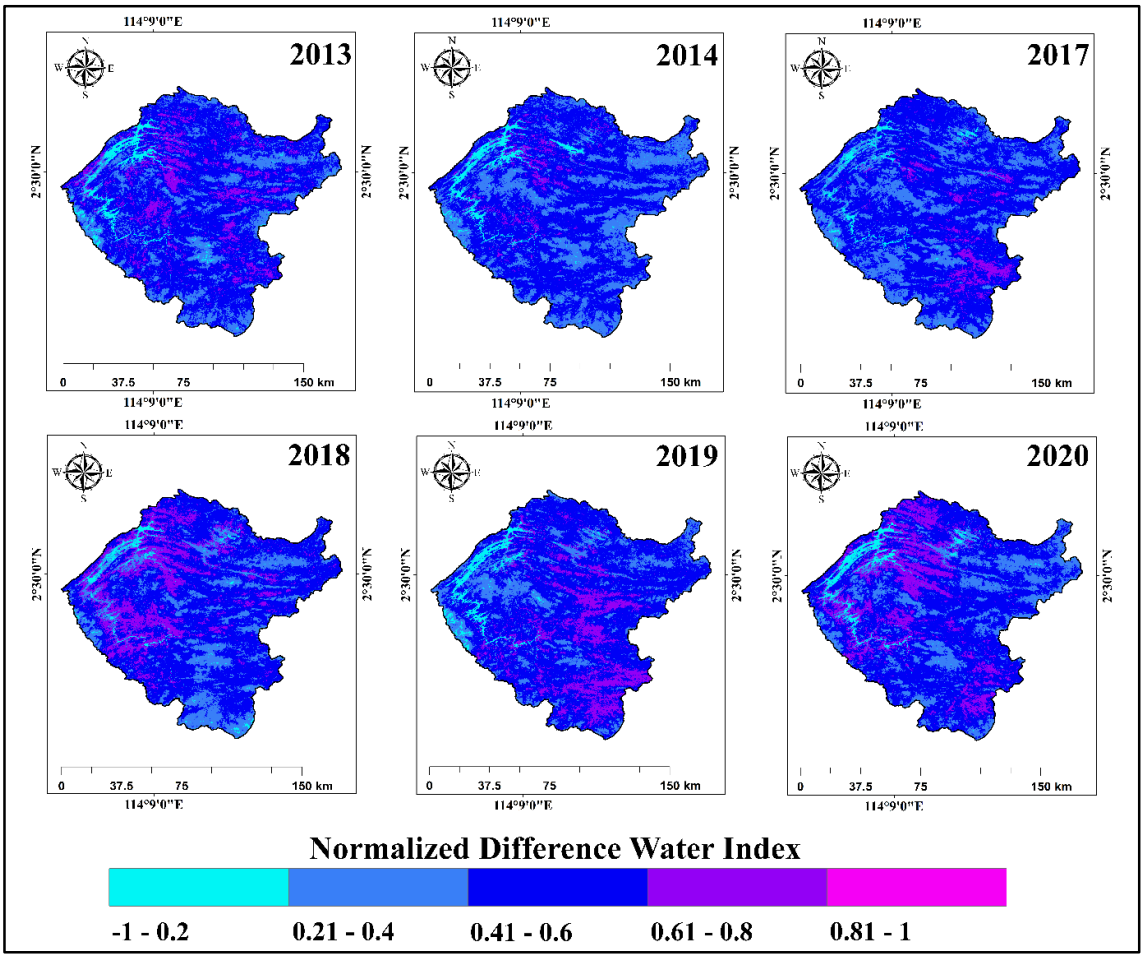

Figure. 5 (c). Temporal variations of the study area's annual mean normalized difference water index (2013, 2014, 2017, 2018, 2019, and 2020).

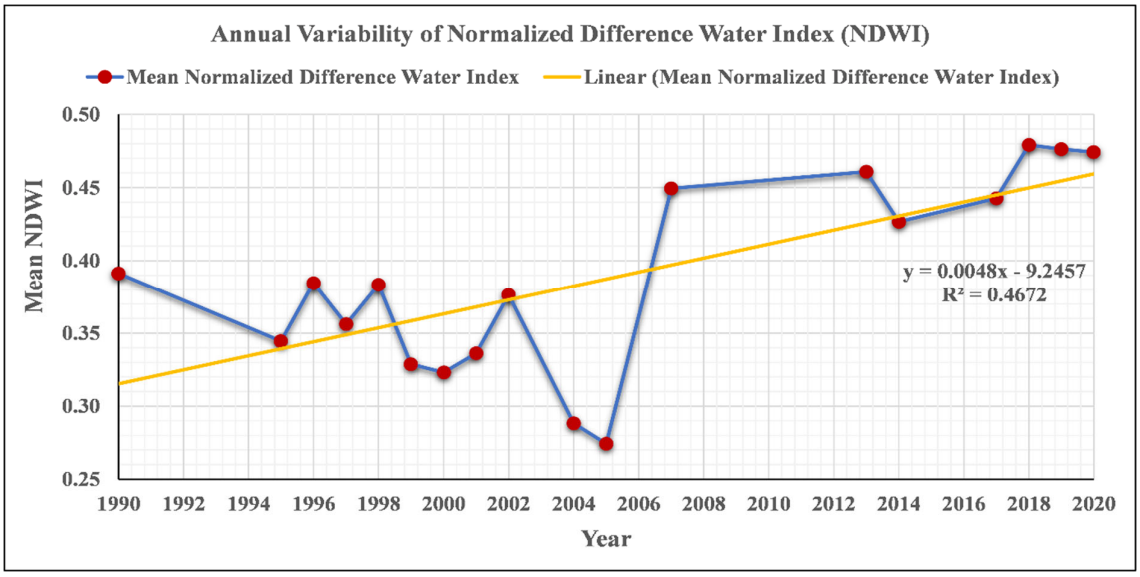

Figure. 5 (d). Annual variability of normalized difference water index from 1990 to 2020.

306 **3.4 Correlation among annual mean NDVI, NDWI, LST, Temperature, and Rainfall**

307 Pearson Correlation among annual mean NDVI, NDWI, LST, temperature, and rainfall
308 was assessed using XLSTAT statistical tool. Table 1 shows the Pearson correlation matrix of
309 the abovementioned variables. Table 1 shows that the NDVI and NDWI significantly correlate
310 with a Pearson correlation matrix (r) of 0.99. A negative relationship between LST and NDVI
311 is found with (r) of 0.30. A weak relationship with (r) of 0.36 between LST and NDWI is also
312 observed. The correlation between annual mean temperature and land surface temperature is
313 found at (r) of 0.39. A negative relation (r) of -0.09 between annual mean rainfall and land
314 surface temperature is observed. Furthermore, a correlation is observed between the annual
315 mean temperature and NDWI (r) of 0.50 and the annual mean temperature and NDVI (r) of
316 0.46. In contrast, a negative relation between annual mean rainfall and other variables is found.

317 Table 2 represents the statistical correlation of annual mean LST with annual mean
318 NDVI with a coefficient of determination of (R^2) of 0.09 is very weak and considered negative.
319 Thus, as stated by (Yue et al.,2007; Huang & Ye, 2015; Dong et al., 2018), the NDVI of the
320 region decreases with an increase in LST. Annual mean LST and annual mean NDWI also
321 show a weak relation (R^2) of 0.13. Furthermore, annual mean LST and annual mean
322 temperature show a modest relationship with (R^2) of 0.15.

323 In Shanghai, China, Yue et al.,2007 also observed an inverse relationship between the
324 land surface temperature and the NDVI. In the Asansol Durgapur area of West Bengal,
325 Choudhury et al., 2019 recorded a decreasing greenery pattern in response to rising LST. The
326 correlation of LST with NDVI in the Karst area was examined by Dong et al., 2018; they found
327 an inverse relationship between these parameters. Furthermore, Sun et al., 2012 saw a
328 substantial decrease in Beijing's LST in the regions surrounding lakes, waterbodies, etc.

329 The relationship of LST with derived factors like NDVI and NDWI in the Asansol-
330 Durgapur Development Area was discovered by Choudhury et al., 2019; they reported an
331 inverse relationship between these LST and NDVI. Figure 6 displays the correlation matrix of
332 the annual mean NDVI, NDWI, LST, temperature, and rainfall developed using R
333 programming (RStudio).

334 **Table 1.** Pearson Correlation Matrix (r).

Variables	Mean Normalized Difference Vegetation Index	Mean Normalized Difference Water Index	Mean Land Surface Temperature °C	Annual Mean Temperature (°C)	Annual Mean Rainfall (mm)

Mean Normalized Difference Vegetation Index	**1**	**0.9902**	0.3021	0.4642	-0.0283
Mean Normalized Difference Water Index	**0.9902**	**1**	0.3607	**0.5042**	0.0353
Mean Land Surface Temperature °C	0.3021	0.3607	**1**	0.3872	-0.0908
Annual Mean Temperature (°C)	0.4642	**0.5042**	0.3872	**1**	-0.1971
Annual Mean Rainfall (mm)	-0.0283	0.0353	-0.0908	-0.1971	**1**

335 * Values in bold are different from 0 with a significance level of alpha=0.05

336 **Table 2.** Statistical Correlation with Coefficients of Determination (R^2).

Variables	Mean Normalized Difference Vegetation Index	Mean Normalized Difference Water Index	Mean Land Surface Temperature °C	Annual Mean Temperature (°C)	Annual Mean Rainfall (mm)
Mean Normalized Difference Vegetation Index	**1**	0.9806	0.0913	0.2155	0.0008
Mean Normalized Difference Water Index	0.9806	**1**	0.1301	0.2542	0.0012
Mean Land Surface Temperature °C	0.0913	0.1301	**1**	0.1499	0.0082
Annual Mean Temperature (°C)	0.2155	0.2542	0.1499	**1**	0.0388
Annual Mean Rainfall (mm)	0.0008	0.0012	0.0082	0.0388	**1**

337 * Values in bold are different from 0 with a significance level of alpha=0.05

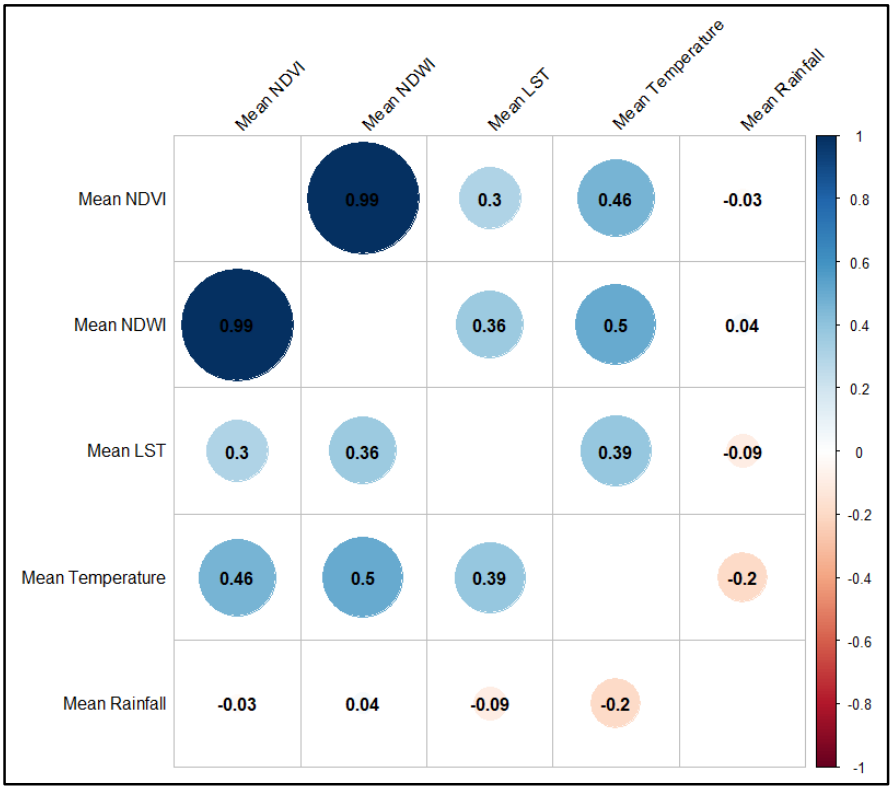

338

339 Figure. 6. Correlation matrix of the annual mean NDVI, NDWI, LST, temperature, and
340 rainfall.

341 **3.5 Trend analysis of rainfall and temperature**

The annual mean temperature and rainfall data of the Bakun-Murum Catchment region from 1990 to 2020 were statistically analyzed using Mann-Kendall trend tests every year to identify temporal changes. The abovementioned climatic parameters are graphically represented in Figure 7. Table 1 represents Mann-Kendall trend test statistics.

The Mann-Kendall trend test for the annual mean temperature series indicates a slightly increasing trend with Sen's slope of 0.03°C/year. From Table 1, it is found that there is a positive trend in the annual mean rainfall patterns, as Sen's slope indicates a yearly increase of 50.58 mm/year. Furthermore, Kendall's tau for annual mean temperature is recorded as 0.50, and for annual mean rainfall, it is 0.27. The p-values (Two-tailed) for both abovementioned parameters are 0.01 and 0.13, respectively. An approximation has been used to compute the p-value.

Table 3. Trend analysis of rainfall and temperature.

Test Statistic	Annual Mean Temperature (°C)	Annual Mean Rainfall (mm)
Kendall's tau	0.50	0.27
p-value (Two-tailed)	0.01	0.13
Sen's slope	0.03	50.58

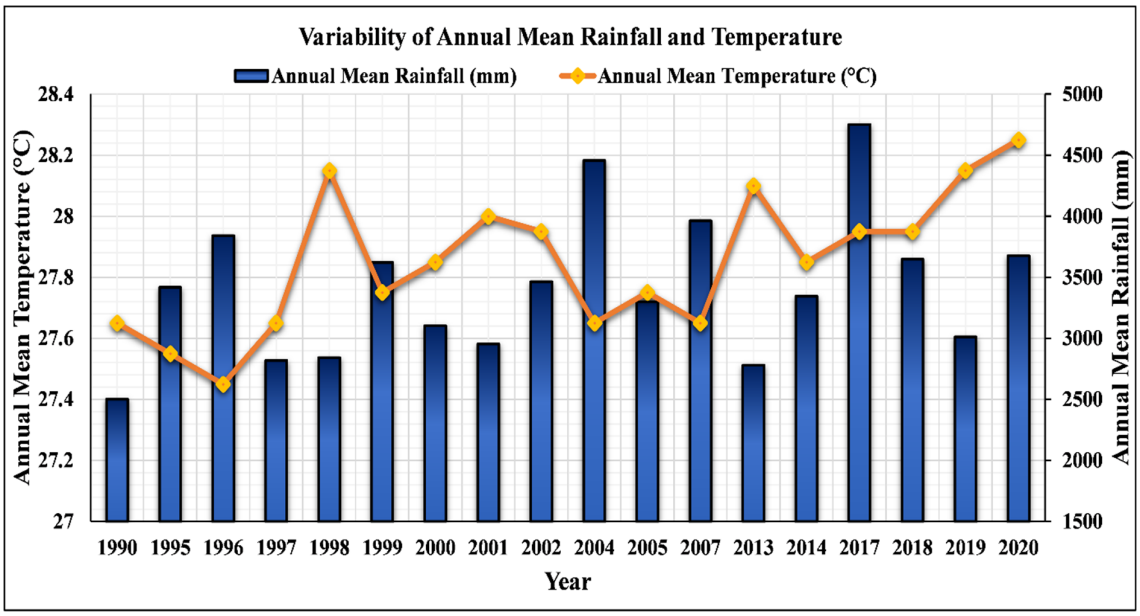

Figure. 7. The trend of annual mean temperature and annual mean rainfall over the selected years.

For the annual mean temperature, as the computed p-value is lower than the significance level alpha=0.05, one should reject the null hypothesis H0 and accept the alternative hypothesis, Ha. The risk of rejecting the null hypothesis H0 while true is lower than 0.58%. The continuity correction has been applied. Ties have been detected in the data, and the appropriate corrections have been applied. Moreover, for the annual mean rainfall, as the computed p-value is more significant than the significance level alpha=0.05, one cannot reject the null hypothesis H0. The risk of rejecting the null hypothesis H0 while true is 12.97%. The continuity correction has been applied for this climatic parameter as well.

The tendency of air temperature to increase equally affects the LST. (Hu et al., 2019; Ali et al., 2020; Ali et al., 2021; Barreto et al., 2021; Memon et al., 2021) demonstrated that air temperature alone showed 81 to 98 per cent change in LST under the cloudy condition and a cloudless sky.

4. Conclusions

For the last thirty years (1990-2020), variations in the LST of the BM catchment area and its effect on the vegetative cover and water bodies have been studied. The research showed that the study area's LST increased by an average of 1.06°C over the last thirty years. The temporal variations in the region's NDVI showed a maximum NDVI of 0.48 in 2018 and 2019, respectively, followed by an NDVI of 0.47 in 2020. In the year 2005, the lowermost NDVI of 0.27 was found. In addition, the region's temporal NDWI variance recorded the highest NDWI of 0.48 in 2018 and 2019, followed by an NDWI of 0.47 in 2020. In the year 2005, the lowest NDWI of 0.27 was observed. An increase in the NDVI shows an increase in vegetation, while an increase in the NDWI shows an increasing amount of water bodies.

An inverse relationship between LST and NDVI is found with (r) of 0.30. An opposite relationship with (r) of 0.36 between LST and NDWI is also observed. Furthermore, an inverse correlation is observed between annual mean temperature and NDWI (r) of 0.50 and annual mean temperature and NDVI (r) of 0.46. At the same time, a negative relation between annual mean rainfall and other variables is found. The statistical correlation of annual mean LST with annual mean NDVI with a coefficient of determination of (R^2) of 0.09 is very weak and considered negative.

In comparison, annual mean LST and annual mean NDWI show an inverse relation (R^2) of 0.13. Moreover, annual mean temperature and annual mean NDVI also indicate a bad relationship with (R^2) of 0.2155; for annual mean temperature and annual mean NDWI, it is

recorded as (R^2) of 0.2542. The Mann-Kendall trend test for the annual mean temperature series indicates a slightly increasing trend with Sen's slope of 0.03°C/year. It is found that there is a positive trend in the annual mean rainfall patterns, as Sen's slope indicates a yearly increase of 50.58 mm/year.

Research studies like this current work are essential to guide policymakers to take steps to mitigate the adverse environmental effects of climate change and human-induced changes (land-use changes). This study corroborates that a significant difference in vegetation cover and surface water bodies occurred during the last three decades, which calls for the concerned authorities' immediate attention to mitigate the negative impacts of such changes and safeguard the ecosystem. Such environmental and human-induced problems can be tackled by reducing deforestation and planting trees.

Limitations and Recommendations

Based on this present study, we recommend that future studies consider land use land cover changes (LULC) analysis and assess the impacts of the LST on LULC for those study areas for which the Landsat satellite data is available with cloud covers below the 10% for conducting the proper analysis as our study has some data availability limitations that is why LULC was not considered in this study. For the Bakun-Murum Catchment region, the available Landsat satellite data for the LULC analysis have cloud covers over 20% from 1990 to 2020. Therefore, we recommend that advanced machine learning and remote sensing techniques be applied to clear the cloud covers from the abovementioned Landsat satellite images for future studies.

Conflicts of Interest: The authors declare no conflict of interest.

References

Ahmad, I., Zhang, F., Tayyab, M., Anjum, M.N., Zaman, M., Liu, J., Farid, H.U. and Saddique, Q., 2018. Spatiotemporal analysis of precipitation variability in annual, seasonal and extreme values over upper Indus River basin. Atmospheric Research, 213, pp.346-360. https://doi.org/10.1016/j.atmosres.2018.06.019.

Alexander, C., 2020. Normalized difference spectral indices and urban land cover as indicators of land surface temperature (LST). International Journal of Applied Earth Observation and Geoinformation, 86, p.102013. https://doi.org/10.1016/j.jag.2019.102013.

Ali, M., de Azevedo, A.R., Marvila, M.T., Khan, M.I., Memon, A.M., Masood, F., Almahbashi, N.M.Y., Shad, M.K., Khan, M.A., Fediuk, R. and Timokhin, R., 2021. The influence of covid-19-induced daily activities on health parameters—a case study in Malaysia. Sustainability, 13(13), p.7465. http://doi.org/10.3390/su13137465.

Ali, M., Room, S., Khan, M.I., Masood, F., Memon, R.A., Khan, R. and Memon, A.M., 2020, December. Assessment of local earthen bricks in perspective of physical and mechanical properties using Geographical Information System in Peshawar, Pakistan. In Structures (Vol. 28, pp. 2549-2561). Elsevier. http://doi.org/10.1016/j.istruc.2020.10.075.

Arfan, M., Lund, J., Hassan, D., Saleem, M. and Ahmad, A., 2019. Assessment of spatial and temporal flow variability of the Indus River. Resources, 8(2), p.103. https://doi.org/10.3390/resources8020103.

Barreto, E.D.S., Stafanato, K.V., Marvila, M.T., de Azevedo, A.R.G., Ali, M., Pereira, R.M.L. and Monteiro, S.N., 2021. Clay ceramic waste as pozzolan constituent in cement for structural concrete. Materials, 14(11), p.2917. http://doi.org/10.3390/ma14112917.

Chan, C.K. and Yao, X., 2008. Air pollution in mega cities in China. Atmospheric environment, 42(1), pp.1-42. https://doi.org/10.1016/j.atmosenv.2007.09.003.

Chen, S., Cai, W., Chen, D., Ren, Y., Li, X., Zhu, Y., Kang, J. and Ruoff, R.S., 2010. Adsorption/desorption and electrically controlled flipping of ammonia molecules on graphene. New Journal of Physics, 12(12), p.125011. https://doi.org/10.1088/1367-2630/12/12/125011.

Chen, X.L., Zhao, H.M., Li, P.X. and Yin, Z.Y., 2006. Remote sensing image-based analysis of the relationship between urban heat island and land use/cover changes. Remote sensing of environment, 104(2), pp.133-146. https://doi.org/10.1016/j.rse.2005.11.016.

Choudhury, D., Das, K. and Das, A., 2019. Assessment of land use land cover changes and its impact on variations of land surface temperature in Asansol-Durgapur Development Region. The Egyptian Journal of Remote Sensing and Space Science, 22(2), pp.203-218. https://doi.org/10.1016/j.ejrs.2018.05.004.

Coolbaugh, M.F., Kratt, C., Fallacaro, A., Calvin, W.M. and Taranik, J.V., 2007. Detection of geothermal anomalies using advanced spaceborne thermal emission and reflection radiometer (ASTER) thermal infrared images at Bradys Hot Springs, Nevada, USA. Remote Sensing of Environment, 106(3), pp.350-359. https://doi.org/10.1016/j.rse.2006.09.001.

Crawford, B., Kasmidi, M., Korompis, F. and Pollnac, R.B., 2006. Factors influencing progress in establishing community-based marine protected areas in Indonesia. Coastal Management, 34(1), pp.39-64. https://doi.org/10.1080/08920750500379300.

Dagliyar, A., Avdan, U., Demircioglu Yildiz, N. and Nefeslioglu, H.A., 2015, April. Determination of land surface temperature by using Landsat 8 TIRS: A case study in Erzurum, Turkey. In EGU General Assembly Conference Abstracts (p. 11007).

Daou, I., Mariko, A., Rasmus, F., Menenti, M., Kourosh, K., Maïga, H.B. and Maïga, S.M., 2012. Estimation and Mapping of Land Surface Temperature From AATSR Images And GIS: A Case Study In Kolondieba-Tiendaga Basin In Sudano-Sahelian Climate, Mali. International Journal of Computational Engineering Research (IJCER), 2 (5), 2012.

Das, D.N., Mondal, A. and Guha, S., 2013. Change in mangrove forest cover and deltaic islands in sundarban areas of West Bengal: a temporal analyses using NCI technique on LANDSAT TM5 data. Climate Change and Environment, Scientific Publisher, pp.113-127.

Dash, P., Göttsche, F.M., Olesen, F.S. and Fischer, H., 2002. Land surface temperature and emissivity estimation from passive sensor data: Theory and practice-current trends. International Journal of remote sensing, 23(13), pp.2563-2594. https://doi.org/10.1080/01431160110115041.

Dong, F., Chen, J. and Yang, F., 2018. A study of land surface temperature retrieval and thermal environment distribution based on landsat-8 in Jinan City. In IOP Conference Series: Earth and Environmental Science (Vol. 108, No. 4, p. 042008). IOP Publishing. http://doi.org/10.1088/1755-1315/108/4/042008.

Douglas, J. and Aochi, H., 2008. A survey of techniques for predicting earthquake ground motions for engineering purposes. Surveys in geophysics, 29(3), pp.187-220. https://doi.org/10.1007/s10712-008-9046-y.

Du, S., Xiong, Z., Wang, Y.C. and Guo, L., 2016. Quantifying the multilevel effects of landscape composition and configuration on land surface temperature. Remote Sensing of Environment, 178, pp.84-92. https://doi.org/10.1016/j.rse.2016.02.063.

Elnashar, A., Abbas, M., Sobhy, H. and Shahba, M., 2021. Crop water requirements and suitability assessment in arid environments: A new approach. Agronomy, 11(2), p.260. https://doi.org/10.3390/agronomy11020260.

480 Ermida, S.L., Soares, P., Mantas, V., Göttsche, F.M. and Trigo, I.F., 2020. Google earth engine
481 open-source code for land surface temperature estimation from the landsat series. Remote
482 Sensing, 12(9), p.1471. https://doi.org/10.3390/rs12091471.

483 Eskandari, A., De Rosa, R. and Amini, S., 2015. Remote sensing of Damavand volcano (Iran)
484 using Landsat imagery: Implications for the volcano dynamics. Journal of Volcanology and
485 Geothermal Research, 306, pp.41-57. https://doi.org/10.1016/j.jvolgeores.2015.10.001.

486 Fang, L., Zhan, X., Hain, C.R., Yin, J., Liu, J. and Schull, M.A., 2018. An assessment of the
487 impact of land thermal infrared observation on regional weather forecasts using two different
488 data assimilation approaches. Remote sensing, 10(4), p.625.
489 https://doi.org/10.3390/rs10040625.

490 Ferrelli, F., Huamantinco Cisneros, M.A., Delgado, A.L. and Piccolo, M.C., 2018. Spatial and
491 temporal analysis of the LST-NDVI relationship for the study of land cover changes and their
492 contribution to urban planning in Monte Hermoso, Argentina.
493 https://doi.org/10.5565/rev/dag.355.

494 Gao, C., Jiang, X., Li, Z.L. and Nerry, F., 2013. Comparison of the Thermal Sensors of SEVIRI
495 and MODIS for LST Mapping. In Thermal Infrared Remote Sensing (pp. 233-252). Springer,
496 Dordrecht. https://doi.org/10.1007/978-94-007-6639-6_12.

497 Ghobadi, Y., Pradhan, B., Shafri, H.Z.M. and Kabiri, K., 2015. Assessment of spatial
498 relationship between land surface temperature and landuse/cover retrieval from multi-temporal
499 remote sensing data in South Karkheh Sub-basin, Iran. Arabian Journal of Geosciences, 8(1),
500 pp.525-537. https://doi.org/10.1007/s12517-013-1244-3.

501 Govil, H., Guha, S., Diwan, P., Gill, N. and Dey, A., 2020. Analyzing linear relationships of
502 LST with NDVI and MNDISI using various resolution levels of Landsat 8 OLI and TIRS data.
503 In Data Management, Analytics and Innovation (pp. 171-184). Springer, Singapore.
504 https://doi.org/10.1007/978-981-32-9949-8_13.

505 Govil, H., Guha, S., Dey, A. and Gill, N., 2019. Seasonal evaluation of downscaled land surface
506 temperature: A case study in a humid tropical city. Heliyon, 5(6), p.e01923.
507 https://doi.org/10.1016/j.heliyon.2019.e01923.

508 Grimm, N.B., Faeth, S.H., Golubiewski, N.E., Redman, C.L., Wu, J., Bai, X. and Briggs, J.M.,
509 2008. Global change and the ecology of cities. science, 319(5864), pp.756-760.
510 https://doi.org/10.1126/science.1150195.

511 Guha, S., Govil, H., Dey, A. and Gill, N., 2020. Analyzing the capability of NCI technique in
512 change detection using high-and medium-resolution multispectral data. In Geoecology of
513 Landscape Dynamics (pp. 133-147). Springer, Singapore. https://doi.org/10.1007/978-981-15-
514 2097-6_10.

515 Hale, R.C., Gallo, K.P., Tarpley, D. and Yu, Y., 2011. Characterization of variability at in situ
516 locations for calibration/validation of satellite-derived land surface temperature data. Remote
517 Sensing Letters, 2(1), pp.41-50. https://doi.org/10.1080/01431161.2010.490569.

518 He, B.J., Zhao, Z.Q., Shen, L.D., Wang, H.B. and Li, L.G., 2019. An approach to examining
519 performances of cool/hot sources in mitigating/enhancing land surface temperature under
520 different temperature backgrounds based on landsat 8 image. Sustainable Cities and Society,
521 44, pp.416-427. https://doi.org/10.1016/j.scs.2018.10.049.

522 Hu, G., Zhao, L., Li, R., Wu, X., Wu, T., Zhu, X., Pang, Q., yue Liu, G., Du, E., Zou, D. and
523 Hao, J., 2019. Simulation of land surface heat fluxes in permafrost regions on the Qinghai-
524 Tibetan Plateau using CMIP5 models. Atmospheric Research, 220, pp.155-168.
525 http://doi.org/10.1016/j.atmosres.2019.01.006.

526 Huang, C. and Ye, X., 2015. Spatial modeling of urban vegetation and land surface
527 temperature: A case study of Beijing. Sustainability, 7(7), pp.9478-9504.
528 https://doi.org/10.3390/su7079478.

529 Huang, S., Taniguchi, M., Yamano, M. and Wang, C.H., 2009. Detecting urbanization effects
530 on surface and subsurface thermal environment—A case study of Osaka. Science of the total
531 environment, 407(9), pp.3142-3152. https://doi.org/10.1016/j.scitotenv.2008.04.019.

532 Hussain, M., Yusof, K.W., Mustafa, M.R.U., Mahmood, R. and Jia, S., 2018. Evaluation of
533 CMIP5 models for projection of future precipitation change in Bornean tropical rainforests.
534 Theoretical and Applied Climatology, 134(1), pp.423-440. https://doi.org/10.1007/s00704-
535 017-2284-5.

536 Karnieli, A., Agam, N., Pinker, R.T., Anderson, M., Imhoff, M.L., Gutman, G.G., Panov, N.
537 and Goldberg, A., 2010. Use of NDVI and land surface temperature for drought assessment:

538 Merits and limitations. Journal of climate, 23(3), pp.618-633.
539 https://doi.org/10.1175/2009JCLI2900.1.

540 Khandelwal, S., Goyal, R., Kaul, N. and Mathew, A., 2018. Assessment of land surface
541 temperature variation due to change in elevation of area surrounding Jaipur, India. The
542 Egyptian Journal of Remote Sensing and Space Science, 21(1), pp.87-94.
543 https://doi.org/10.1016/j.ejrs.2017.01.005.

544 Li, Z.L., Tang, B.H., Wu, H., Ren, H., Yan, G., Wan, Z., Trigo, I.F. and Sobrino, J.A., 2013.
545 Satellite-derived land surface temperature: Current status and perspectives. Remote sensing of
546 environment, 131, pp.14-37. https://doi.org/10.1016/j.rse.2012.12.008.

547 Liu, H., Zhan, Q., Yang, C. and Wang, J., 2018. Characterizing the spatio-temporal pattern of
548 land surface temperature through time series clustering: Based on the latent pattern and
549 morphology. Remote sensing, 10(4), p.654. https://doi.org/10.3390/rs10040654.

550 Maffei, C., Alfieri, S.M. and Menenti, M., 2018. Relating spatiotemporal patterns of forest fires
551 burned area and duration to diurnal land surface temperature anomalies. Remote Sensing,
552 10(11), p.1777. https://doi.org/10.3390/rs10111777.

553 Martin, M.A., Ghent, D., Pires, A.C., Göttsche, F.M., Cermak, J. and Remedios, J.J., 2019.
554 Comprehensive in situ validation of five satellite land surface temperature data sets over
555 multiple stations and years. Remote Sensing, 11(5), p.479. https://doi.org/10.3390/rs11050479.

556 McFeeters, S.K., 2013. Using the normalized difference water index (NDWI) within a
557 geographic information system to detect swimming pools for mosquito abatement: a practical
558 approach. Remote Sensing, 5(7), pp.3544-3561. https://doi.org/10.3390/rs5073544.

559 McFeeters, S.K., 1996. The use of the Normalized Difference Water Index (NDWI) in the
560 delineation of open water features. International journal of remote sensing, 17(7), pp.1425-
561 1432. https://doi.org/10.1080/01431169608948714.

562 Memon, A.M., Sutanto, M.H., Napiah, M., Yusoff, N.I.M., Memon, R.A., Al-Sabaeei, A.M.
563 and Ali, M., 2021. Physicochemical, rheological and morphological properties of bitumen
564 incorporating petroleum sludge. Construction and Building Materials, 297, p.123738.
565 http://doi.org/10.1016/j.conbuildmat.2021.123738.

566 Meng, X., Cheng, J. and Liang, S., 2017. Estimating land surface temperature from Feng Yun-
567 3C/MERSI data using a new land surface emissivity scheme. Remote Sensing, 9(12), p.1247.
568 https://doi.org/10.3390/rs9121247.

569 Mia, M.B., Fujimitsu, Y. and Nishijima, J., 2018. Monitoring of thermal activity at the
570 Hatchobaru–Otake geothermal area in Japan using multi-source satellite images—With
571 comparisons of methods, and solar and seasonal effects. Remote Sensing, 10(9), p.1430.
572 https://doi.org/10.3390/rs10091430.

573 Mondal, A., Guha, S., Mishra, P.K. and Kundu, S., 2011. Land use/Land cover changes in
574 Hugli Estuary using Fuzzy CMean algorithm. International Journal of Geomatics and
575 Geosciences, 2(2), pp.613-626.

576 Nakisa, M., Maimun, A., Ahmed, Y.M., Behrouzi, F., Koto, J., Priyanto, A., Sian, A.Y. and
577 Ghazanfari, S.A., 2014. Ship navigation effect on sedimentation in restricted waterways. Jurnal
578 Teknologi, 69(7). https://doi.org/10.11113/jt.v69.3279.

579 Naughton, J. and McDonald, W., 2019. Evaluating the variability of urban land surface
580 temperatures using drone observations. Remote Sensing, 11(14), p.1722.
581 https://doi.org/10.3390/rs11141722.

582 Nimish, G., Bharath, H.A. and Lalitha, A., 2020. Exploring temperature indices by deriving
583 relationship between land surface temperature and urban landscape. Remote Sensing
584 Applications: Society and Environment, 18, p.100299.
585 https://doi.org/10.1016/j.rsase.2020.100299.

586 Oad, V.K., Dong, X., Arfan, M., Kumar, V., Mohsin, M.S., Saad, S., Lü, H., Azam, M.I. and
587 Tayyab, M., 2020. Identification of Shift in Sowing and Harvesting Dates of Rice Crop (L.
588 Oryza sativa) through Remote Sensing Techniques: A Case Study of Larkana District.
589 Sustainability, 12(9), p.3586. https://doi.org/10.3390/su12093586.

590 Oad, V.K., Mustafa, M.R.U., Takaijudin, H.B., Nabi, G. and Hussain, M., 2020, November.
591 Monitoring trends of land use and land cover changes in rajang river basin. In 2020 Second
592 International Sustainability and Resilience Conference: Technology and Innovation in
593 Building Designs (51154) (pp. 1-8). IEEE.
594 https://doi.org/10.1109/IEEECONF51154.2020.9319939.

595 Patz, J.A., Campbell-Lendrum, D., Holloway, T. and Foley, J.A., 2005. Impact of regional
596 climate change on human health. Nature, 438(7066), pp.310-317.
597 https://doi.org/10.1038/nature04188.

598 Rajendran, P. and Mani, K., 2015. Estimation of spatial variability of land surface temperature
599 using Landsat 8 imagery. International Journal of Engineering and Science, 11(4), pp.19-23.

600 Sekertekin, A. and Arslan, N., 2019. Monitoring thermal anomaly and radiative heat flux using
601 thermal infrared satellite imagery–A case study at Tuzla geothermal region. Geothermics, 78,
602 pp.243-254. https://doi.org/10.1016/j.geothermics.2018.12.014.

603 Sekertekin, A., Kutoglu, S.H. and Kaya, S., 2016. Evaluation of spatio-temporal variability in
604 Land Surface Temperature: A case study of Zonguldak, Turkey. Environmental monitoring
605 and assessment, 188(1), pp.1-15. https://doi.org/10.1007/s10661-015-5032-2.

606 Simwanda, M., Ranagalage, M., Estoque, R.C. and Murayama, Y., 2019. Spatial analysis of
607 surface urban heat islands in four rapidly growing African cities. Remote Sensing, 11(14),
608 p.1645. https://doi.org/10.3390/rs11141645.

609 Solangi, G. S., Siyal, A. A., & Siyal, P. (2019). Spatiotemporal dynamics of land surface
610 temperature and its impact on the vegetation. Civil Engineering Journal, 5(8), 1753-1763.
611 https://doi.org/10.28991/cej-2019-03091368

612 Sruthi, S. and Aslam, M.M., 2015. Agricultural drought analysis using the NDVI and land
613 surface temperature data; a case study of Raichur district. Aquatic Procedia, 4, pp.1258-1264.
614 https://doi.org/10.1016/j.aqpro.2015.02.164.

615 Sultana, S. and Satyanarayana, A.N.V., 2020. Assessment of urbanization and urban heat island
616 intensities using landsat imageries during 2000–2018 over a sub-tropical Indian City.
617 Sustainable Cities and Society, 52, p.101846. https://doi.org/10.1016/j.scs.2019.101846.

618 Sun, R., Chen, A., Chen, L. and Lü, Y., 2012. Cooling effects of wetlands in an urban region:
619 The case of Beijing. Ecological Indicators, 20, pp.57-64.
620 http://doi.org/10.1016/j.ecolind.2012.02.006.

621 Tayyab, M., Dong, X., Ahmad, I., Zahra, A., Zhou, J., Zeng, X. and Shakoor, A., 2019.
622 Identifying Half-Century Precipitation Trends in a Chinese Lake Basin. Polish Journal of
623 Environmental Studies, 28(3). https://doi.org/10.15244/pjoes/85674.

624 Townshend, J.R.G., Justice, C.O., Skole, D., Malingreau, J.P., Cihlar, J., Teillet, P., Sadowski,
625 F.A. and Ruttenberg, S., 1994. The 1 km resolution global data set: needs of the International
626 Geosphere Biosphere Programme. International Journal of Remote Sensing, 15(17), pp.3417-
627 3441. https://doi.org/10.1080/01431169408954338.

628 Wan, Z. and Dozier, J., 1996. A generalized split-window algorithm for retrieving land-surface
629 temperature from space. IEEE Transactions on geoscience and remote sensing, 34(4), pp.892-
630 905. https://doi.org/10.1109/36.508406.

631 Waseem, M., Ahmad, I., Mujtaba, A., Tayyab, M., Si, C., Lü, H. and Dong, X., 2020.
632 Spatiotemporal dynamics of precipitation in southwest arid-agriculture zones of Pakistan.
633 Sustainability, 12(6), p.2305. https://doi.org/10.3390/su12062305.

634 Wen, L., Peng, W., Yang, H., Wang, H., Dong, L. And Shang, X., 2017. An analysis of land
635 surface temperature (LST) and its influencing factors in summer in western Sichuan Plateau:
636 A case study of Xichang City. Remote Sensing for Land & Resources, (2), pp.207-214.
637 https://doi.org/10.6046/gtzyyg.2017.02.30.

638 Yuan, X., Wang, W., Cui, J., Meng, F., Kurban, A. and De Maeyer, P., 2017. Vegetation
639 changes and land surface feedbacks drive shifts in local temperatures over Central Asia.
640 Scientific Reports, 7(1), pp.1-8. https://doi.org/10.1038/s41598-017-03432-2.

641 Yue, W., Xu, J., Tan, W. and Xu, L., 2007. The relationship between land surface temperature
642 and NDVI with remote sensing: application to Shanghai Landsat 7 ETM+ data. International
643 journal of remote sensing, 28(15), pp.3205-3226. http://doi.org/10.1080/01431160500306906.

644 Zhou, D., Xiao, J., Bonafoni, S., Berger, C., Deilami, K., Zhou, Y., Frolking, S., Yao, R., Qiao,
645 Z. and Sobrino, J.A., 2018. Satellite remote sensing of surface urban heat islands: Progress,
646 challenges, and perspectives. Remote Sensing, 11(1), p.48.
647 https://doi.org/10.3390/rs11010048.